Transparent Watermarking using Bidirectional Imaging

Kristin J. Dana
Gabriela Livescu *
Raghunand Makonahalli
Department of Electrical and Computer Engineering
Rutgers University

Abstract

We present a method for transparent watermarking using a custom bidirectional imaging device. The two innovative concepts of our approach are reflectance coding and multiview imaging. In reflectance coding, information is embedded in the angular space of the bidirectional reflectance distribution function (BRDF) and this information can vary at each surface point. In order to achieve a transparent watermark, reflectance coding is implemented using a spatial variation of the Brewster angle. The novel multiview imaging method measures the reflectance over a range of viewing and illumination angles in order to instantly reveal the unknown Brewster angle. Unlike typical in-lab measurements of the Brewster angle or the refractive index, this method does not require accurate prior knowledge of the surface normal so that imaging in non-lab conditions is feasible. Furthermore, a range of incident angles are examined simultaneously, eliminating the need for scanning incidence angles. The approach is well-suited for transparent watermarking where the observer cannot see the watermark because it is comprised of spatial variations of refractive index. The transparency and angular coding of the watermark has great utility in deterring counterfeit attempts. In this paper, we present the imaging device and demonstrate it's effectiveness in detecting and measuring changes in refractive index. This device acts as the decoder in a transparent watermark system.

1. Introduction

Physical watermarks such as raised seals and standard watermark labels enable the authentication of important financial and legal documents. While digital watermarking has become important for tracing documents in cyberspace, the real world still requires verification of physical documents such as licenses, passports, and birth certificates. Physical watermarking is therefore a distinct field with goals and methods that are different from digital watermarking or steganography. Barcoding is a good example of an efficient marking technique, but a barcode is clearly visible and can be easily duplicated. Because of advances in printing technologies, any pattern that is visible can be duplicated, although with varying levels of difficulty. Even markings that aren't visible, such and infrared "invisible inks" can be reverse engineered using commercial infrared cameras. The ideal patterns should not visible by eye or by commercially available cameras.

We present a new imaging concept that uses multiview imaging to estimate the local Brewster angle so that patterns can be comprised of a spatially varying refractive index in a transparent coating. Consider the standard watermark pattern on a document today. To view the watermark, the paper is held at a particular angle and then the pattern is revealed. This notion of angular dependence of the appearance of the reflectance of the pattern is very important. But for current watermarks, all of the pattern is revealed at the *same* angle. For our approach, each point of the pattern is revealed at a *different* angle, so no tilt of the surface reveals the pattern.

The two innovative concepts of our approach are: (1) multiview imaging and (2) reflectance coding. The new multiview imaging device is a bidirectional imager that measures the reflectance over a range of viewing and illumination angles in order to instantly reveal the unknown Brewster angle. Each point in the pattern has a different bidirectional reflectance distribution function (BRDF). The BRDF is the radiance as a function of viewing and illumination direction and can be denoted by $f(\theta_v, \phi_v, \theta_i\, \phi_i)$, where θ_v, ϕ_v are the polar and azimuth of the viewing direction and θ_i, ϕ_i are the polar and azimuth angles of the illumination direction. Therefore, the BRDF for a single surface point is a four dimensional function (for a specific wavelength) and can be utilized for storing information. Information can be embedded at different angular positions at each surface point. We use the term "reflectance coding" for this process of storing information in the angular space

*Dr. Livescu was a visiting professor during this work.

978-1-4244-3993-5/09/$25.00 ©2009 IEEE

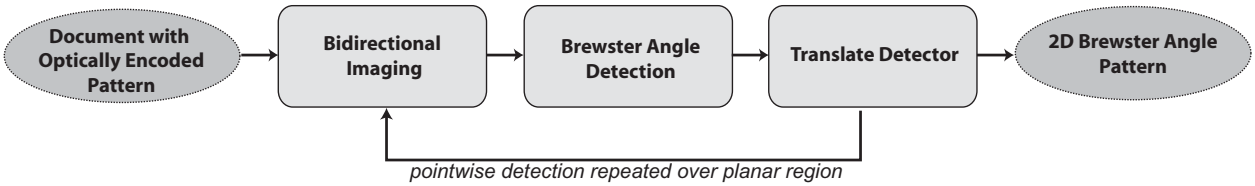

Figure 1. System Overview. Bidirectional imaging enables the detection of the Brewster angle at a surface point. The spatially varying Brewster angle is detected by translating the detector over a two dimensional planar region.

of the BRDF. The overall pattern cannot be viewed at any one angle, and the angular positions for viewing can be a secure code that is unknown to the users (document owner or verifier).

The bidirectional imager is a modification of the mirror-based device [1, 2] that uses a concave parabolic mirror to get multiple views of a single image point. This device has significant advantages because multiple reflectance angles are measured simultaneously without moving the light source or imaging sensor as in more complex gonioreflectometers. Instead, each point on the mirror senses light from the same surface point, but from a different angle. By imaging the entire mirror surface, a large range of reflectance angles are viewed simultaneously. By using a beam splitter, the same mirror can illuminate the surface point at a range angles.

In prior methods for estimating the Brewster angle [3, 4, 5] a range of incidence angles are scanned and the resultant reflectance is analyzed. While these classic methods for estimating Brewster angle and refractive index are used to this day [6, 7], they suffer from the drawback that the exact surface orientation must be known. This requirement is unrealistic for real-world documents, cards and booklets which are often not precisely planar due to folds and bends. In our method, a large range of viewing angles are measured, so it is not necessary to know the surface normal a priori. In traditional methods for estimating the brewster angle, the illuminant and detector must be systematically reoriented to all possible incidence and exitance angles until the minimum reflectance is recorded. Our imaging approach enables instant estimation of the Brewster angle without scanning the angular space.

Properties of the Brewster angle have been used in other applications, most notably in Brewster angle microscopy (BAM) [8, 9, 10]. This microscopy technique allows the direct observation of ultra thin organic films on transparent dielectric substrates. While our approach uses the Brewster angle property of minimum reflectance, it differs from BAM in several fundamentally important ways. In BAM, the Brewster angle of the substrate is known and the illumination angle is fixed to this known Brewster angle. In our approach, the unknown Brewster angle is detected. This detection is possible because the bidirectional imager illuminates and views a large range of angles simultaneously.

Other prior approaches to advanced watermarking use markings that are outside the visible spectrum as the authentication method. Several manufacturers offer invisible inks that use techniques such as ultraviolet fluorescence and infrared absorption. However, these methods are only a small advancement over visible watermarks and detectors for reading such markings are commercially available. Other methods for document security are described in recent surveys [11, 12] and include holograms [13, 14], intaglio printing [15, 16], and zero-order micrograting [17]. These techniques have the advantage that they cannot be copied by simple scanning. The printing of paper currency is designed so that standard copiers and scanners cannot duplicate the bills [18, 19]. For example, lines and circles are spaced so that standard copying will produce interference patterns. However, the patterns are visible by eye, and can be duplicated with a sufficiently sophisticated technique.

2. Reflectance Coding

Information can be stored in the reflectance pattern of materials in a variety of ways. Our method is based on the optical reflection properties of transparent materials illuminated with polarized light. If the polarization is parallel to the plane of incidence, and the angle of incidence is equal to the Brewster angle, no reflection occurs from the flat surface of these materials. This method of reflectance coding is illustrated in Figure 1. The pattern consists of a spatially varying deposition of materials which differ in refractive index. In this paper we assume that the pattern is given, i.e. the actual method of generating the pattern by depositing transparent media of different refractive indices is not addressed. Bidirectional imaging reveals the unknown Brewster angle in a single multiview image, then the mirror component of the detector is translated to the neighboring surface point and this process is repeated over a 2D grid. The resulting 2D pattern of Brewster angles comprises a code to be used for authentication.

The physical phenomenon of Brewster angle reflection is well known. For a monochromatic, linearly polarized plane wave incident at the planar interface between two materials of refractive indices n_1 and n_2, the reflectivity (ratio

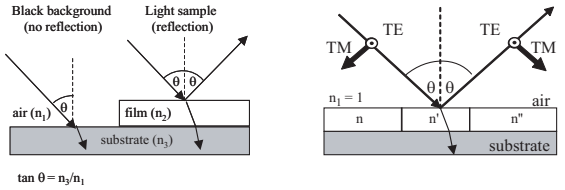

(a) (b)

Figure 2. Illustration of Brewster angle based optical methods. (a) Principle of operation of the Brewster angle microscope. When polarized light is incident at the Brewster angle corresponding to the substrate of refractive index n_3, the reflection is zero, resulting in a black background. The sample of refractive index n_2 has a different Brewster angle, so that its reflection at angle is not zero. In this way, thin transparent films can be made visible on transparent substrates. (b) Principle of operation of our Brewster angle encoded patterns. The pattern can be made of pixels (squares or rectangles) of thin films of different refractive indices on top of the substrate. A plane wave incident at an angle at the interface between air ($n_1 = 1$) and the pattern of thin films ($n_2 = n, n', n''$) can have TE polarization (perpendicular to the plane of incidence, shown with dotted circle) or TM polarization (parallel to the plane of incidence, shown with arrows). We use the TM polarization whose reflection becomes zero at the Brewster angle. Pixels in the pattern appear dark (zero reflection) at the Brewster angles corresponding to their respective indices of refraction. The pattern can be encoded by choosing a certain spatial distribution of the indices of refraction, or equivilantly, a spatial distribution of Brewster angles.

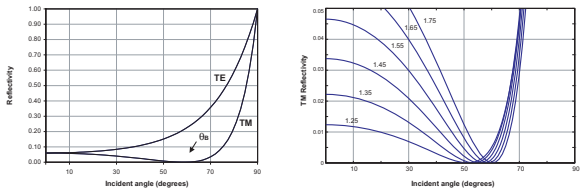

(a) (b)

Figure 3. (a) The ratio between reflected and incident optical powers (reflectivity) is different for the two polarizations. In the case of parallel polarization, the reflectivity becomes zero at the Brewster angle θ_B. (b) The angular dependence of the TM reflectivity and the value of the Brewster angle are determined by the relative refractive index, $n = n_2/n_1$. The curves above correspond to typical values of refractive indices of optically transparent materials The values n used are indicated next to each curve.

between the reflected and incident intensities) can be calculated by using the Fresnel equations [20]. Figure 3-(a) illustrates the results for the TE and TM polarizations. Here TE is the "transverse electric" polarization (the electric is field perpendicular to the plane of incidence), and TM is the "transverse magnetic" polarization (the magnetic field is perpendicular to the plane of incidence, thus the electric field is parallel to the plane of incidence). Let $R(\theta)$ denote the reflectivity in the direction of $-\theta$ as a function of incidence angle θ. For both polarizations, the reflectivity R increases from its normal incidence value

$$R(0) = \left[\frac{(n-1)}{(n+1)}\right]^2 \tag{1}$$

to

$$R\left(\frac{\pi}{2}\right) = 1 \tag{2}$$

at grazing incidence. For the TM polarization, however, the reflectivity becomes zero at the Brewster angle θ_B is given by

$$\theta_B = \tan^{-1}(n). \tag{3}$$

Thus, when TM (or "parallel") polarized light is used, a pattern pixel illuminated under the Brewster angle appears dark. The Brewster angle and the angular dependence of the reflectivity are fully determined by the index of refraction, which is characteristic to the material. Figure 3-(b) illustrates this dependence for values of the refractive index typical to optically transparent materials. Note that the Brewster angle increases for increasing refractive index. The shape of the reflectivity curve in the vicinity of the reflectivity minimum is also strongly dependent on the value of the refractive index. For a given angle of incidence, for example $10°$, the reflectivity can vary by a factor of 4 when the refractive index changes between 1.25 and 1.55.

3. Bidirectional Imaging System

A bidirectional imaging system can measure reflectance as a function of viewing and illumination direction, i.e. $f(\theta_v, \phi_v, \theta_i, \phi_i)$. The viewing direction is specified by the polar and azimuth angles θ_v,ϕ_v respectively. Similarly the illumination direction is specified by θ_i, ϕ_i. In typical bidirectional measurements, the camera and the light source must be positioned in all possible combinations of viewing and illumination directions. For both the light source and camera, the set of all possible directions is a hemisphere above the surface point. Bidirectional imaging is often a difficult task. Typically a rigid dome is constructed or the camera and light source are positioned with robotics. The measurements are quite cumbersome, the space required is problematic and the occlusions of camera or light source compound the difficulties. In prior work [1, 2], a bidirectional imaging device was developed that uses a curved mirror to create a convenient imaging device where multiple views of the same surface point are realized simultaneously. A concave parabolic mirror focuses light to a single point. Therefore, this mirror can be used for convenient orientation of the illumination direction. An incident ray reflecting off the mirror will reach the surface at an angle θ determined by the point of intersection with the mirror as shown in Figure 4. The light reflected from the surface point at

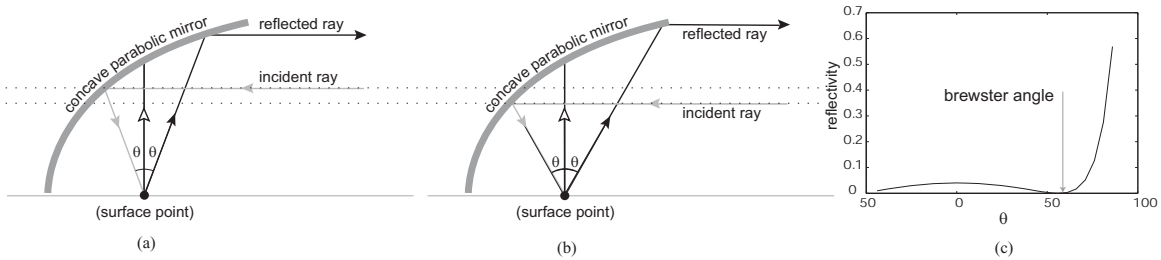

Figure 4. The focusing property of a concave parabolic mirror is exploited to simultaneously measure reflected rays. (a) The mirror is used to direct the incident illumination ray to the sample at the desired angle θ and the reflected ray at angle $-\theta$ is sensed by a CCD camera. (b) By employing a beam splitter and a moving aperture, the incident ray can be translated and consequently the angle θ is varied over the range of interest. (c) The Brewster angle is estimated by finding the minimum reflected light as a function of θ.

a large range of angles is also reflected by the mirror and can be imaged by the camera. The image of the mirror is viewed by a camera with a telecentric lens that is positioned so that its optical axis is parallel to the reflected rays. In this manner, *a single image* corresponds to reflectance measurements at all angles in a partial hemisphere, i.e. the camera captures a *multiview image*. The measured reflectance in this multiview image is from a single surface point. To obtain a measurement of a surface patch for spatially varying reflectance, the concave mirror is translated along the X-Y plane.

Figure 4 illustrates a cross section of the concave parabolic mirror. For a particular illumination angle θ (obtained by a particular position of the illumination aperture) the direction of specular reflection is $-\theta$. Each position of the aperture corresponds to a different incident angle (Figure 4 b). The reflected intensities for each value of θ are recorded and the relationship of the reflection coefficient to θ as illustrated in Figure 4-(c), reveals the Brewster angle. The curve shown in this figure is idealized and the minimum is exactly zero. The location of the minimum will be used as the Brewster angle estimate.

For capturing specular reflection, the sample should be illuminated at angle θ and the reflected ray at angle $-\theta$ should be observed (see Figure 4-(a) and (b)). Since the Brewster angle is not known a priori, multiple θ angles should be tried. With our device, this requirement is easily met by using a slit aperture to pass multiple rays and illuminate a section of the mirror which consequently illuminates the point with multiple angles.

An additional advantage of our imaging device is that angles for a range of azimuth positions are also measured (the concave parabolic mirror images a hemisphere, not a slice of the hemisphere). Consider what happens if the normal of the surface deviates from it's expected position. Because the bidirectional image sees more than just a fixed azimuth, the detection process can be made robust to surface tilts. This is essential in practice since documents are often folded or warped and are not perfectly planar.

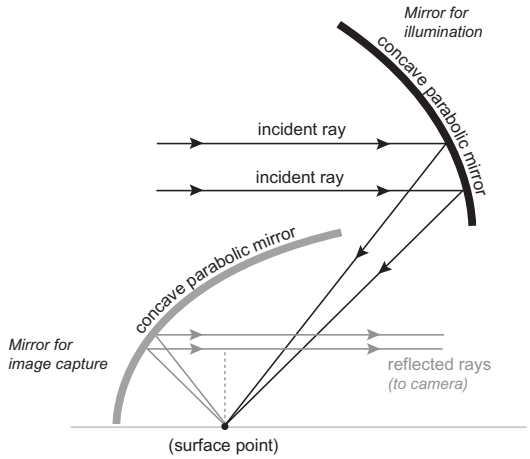

Figure 5. Two mirror configuration. The focii of the two mirrors is coincident. The range of illumination angles between $50^\circ - 60^\circ$ can be achieved. A single mirror could be used if it has a range of $-60^\circ - 60^\circ$ and a beam splitter separates the path of illumination and image capture. However the two mirror arrangement is preferred to avoid the manufacturing costs of a long parabolic mirror.

4. Device Prototype

The bidirectional imager can be made with a single parabolic mirror to both illuminate the mirror and detect light from the mirror as indicated in Figure 4. However, this requires the parabolic mirror to have an equal range of angles about the surface normal. The typical Brewster an-

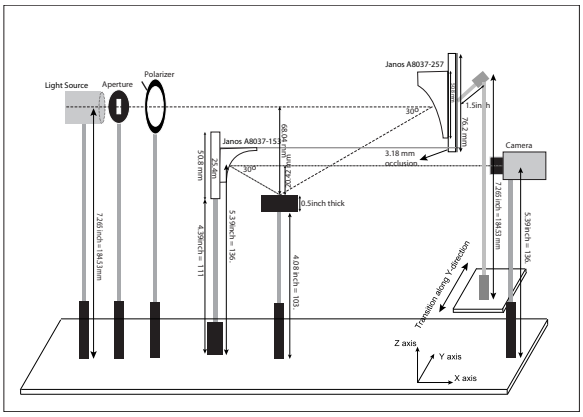

Figure 6. Device prototype diagram.

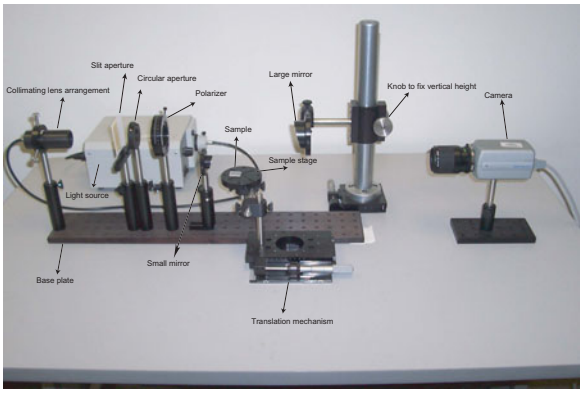

Figure 7. Device prototype.

gles are shown in Figure 3 and are in the range of $50°$ to $60°$. Therefore the range of angles covered by the mirror must extend from $-60°$ to $60°$. However, this relatively large range requires a longer mirror and more manufacturing expense in practice. Instead, we choose to use a two mirror configuration as shown in Figure 5.

An additional advantage of this two mirror configuration is that all the components are aligned along parallel optical axes. This configuration helps in reducing the overall area required for the device setup. The prototype arrangement is shown in Figure 6 and is comprised of a collimated light source quartz halogen light source[1], a slit aperture, a polarizer[2], two concave parabolic mirrors[3] [4], a camera[5] equipped with a telecentric lens[6] and a sample platform. The sample platform can be attached to an automated positioning stage in order to scan a pattern. A single base plate holds all remaining components except the large upper mirror. The post of the upper mirror is placed off axis so that it does not occlude the lower mirror from the camera view.

The photograph of the constructed prototype is shown in Figure 7. The entire device consists of two layers: (1) the illumination layer and (2) the image capture layer. The illumination layer of the device consists of a collimated illumination source, slit aperture, rotating polarizer and a concave parabolic mirror. The slit aperture is placed in front of the collimating lens arrangement to enable multiple illumination angles. The rotating polarizer controls the polarization angle and the upper parabolic mirror reflects the incident rays to the sample point.

The image capture layer consists of the lower parabolic mirror and a CCD camera equipped with a telecentric lens. The light reflected from the surface point intersects the lower parabolic mirror. Since the surface point is coincident with the focus of the lower mirror, the light is reflected by the mirror into a set of parallel rays (see Figure 5). The CCD camera captures the image of the mirror. The camera is equipped with an orthographic or telecentric lens that images the light parallel to the optical axis.

5. Refractive Index Imaging

For each test sample we take 30 images for the same illumination intensity and polarization. These images are averaged to reduce additive image noise. To compensate for the limited dynamic range of the camera we use high dynamic range imaging [21] to obtain the final image. Specifically, we sum three sets of images with the same polarization but varying illumination intensity. The resultant images capture a higher level of detail than the original individual images. Gamma correction is performed to account for the nonlinearities of the camera response. The camera images contain a line of interest corresponding to the reflected light from the slit aperture (See Figure 8). The exact position of the line is unknown (because the sample may not be exactly planar), so a line is fit to the image intensities using linear least squares estimation. Each image pixel corresponds to a known viewing angle, so intensities along this line provide a function $i(\theta)$. The minimum intensity of i occurs at the Brewster angle.

Because the original image contains a circular region of interest and a background, the intensities plotted along the length of the image appear as shown in Figure 9 (top). Notice the intensities are plotted as a function of the pixel coordinates along the length of the image. Each pixel corresponds to an angle of incidence on the sample surface. The part of the plot that corresponds to the mirror area is the section of interest. This section is manually extracted and is referred to as the *measurement curve*.

The measurement curve provides the characteristic information about the sample that has been imaged. We are

[1] USHIO Inc. Tokyo, Japan. Model number - 21V150W
[2] Edmund Optics. Model number - NT47-314
[3] Janos Technology No. A8037-257 (upper mirror)
[4] Janos Technology No. A8037-153 (lower mirror)
[5] DFW-V500 Sony digital color video camera, Chori America Inc.
[6] 55mm telecentric, (Edmund Scientific)

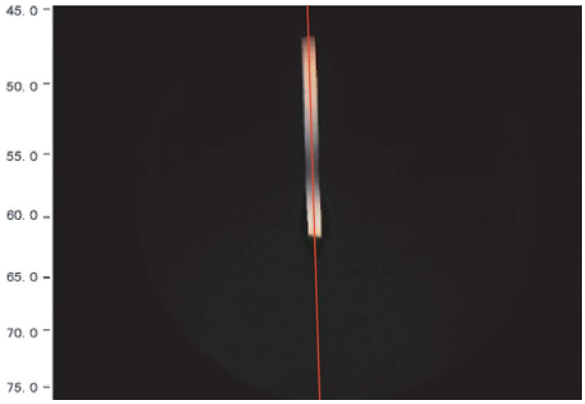

Figure 8. The camera image when the sample is illuminated using a slit aperture. As expected the reflected intensity lies in a line. A fitting procedure is done to extract that the line of interest.

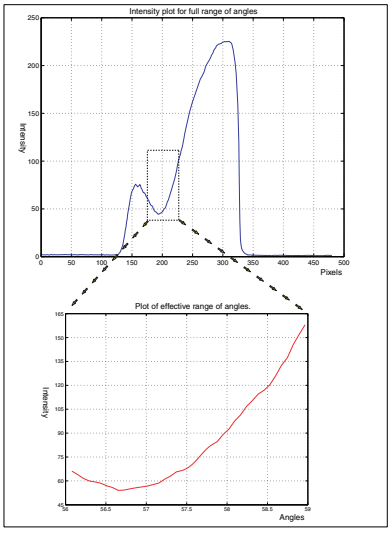

Figure 9. (Top) Intensity values along the entire length of the image (note that the x-axis is in terms of pixel values). The dotted rectangle is the area of interest and is extracted to obtain the measurement curve $i(\theta)$ (Bottom). Finding the minimum of the measurement curve gives the Brewster angle.

interested in both the minima and the shape of these curves in order to estimate the refractive index.

We have employed two methods to estimate the refractive index: (1) the minimum intensity estimate and (2) the nonlinear curve fit. The first method finds the position of the minima, while the other takes the entire measurement curve into consideration.

For the minimum intensity estimate, we find a pixel that corresponds to the minimum intensity in the measurement curve. This pixel is mapped to the corresponding incidence angle θ using the known geometry of the mirror. Consider the glass sample with a measurement curve shown in Figure 9 and with a known refractive index of 1.517. The pixel number 190 has minimum intensity and this maps to and angle of incidence $\theta = 56.6°$ and a refractive index of 1.51 The refractive index n is estimated from θ using the relation,

$$n = \tan\ \theta. \tag{4}$$

Using the minimum intensity pixel we can estimate the refractive index of the sample with good accuracy.

Another way to estimate the refractive index is using non-linear curve fitting techniques. The ideal curve for the curve fitting algorithm is obtained using the relation

$$i = \left(\frac{\cos\ \theta - \sqrt{(1 - \sin^2\ \theta/n^2)}}{\cos\ \theta + \sqrt{(1 - \sin^2\ \theta/n^2)}} \right)^2. \tag{5}$$

For the fitting process, we provide the algorithm with 3 parameters: the initial guess of the refractive index, the scaling factor and the vertical shift value. The algorithm alters these parameters iteratively until a minimum for the error and the estimated refractive index is found. We employ the Levenberg-Marquardt method implemented in Matlab for this purpose.

6. Experiments

Refractive index standards are used to perform experiments designed to check the accuracy of the refractive index estimates that the system produces. We perform the two methods of estimating the refractive index separately and compare them.

Seven samples of known refractive index comprise the test set. One sample is an optical grade glass with a known refractive index equal to 1.517. One of the liquids used is water whose refractive index is known to be 1.33. The remaining 5 liquids have refractive indices ranging from 1.3 to 1.7 with intervals of 0.1.[7] The liquids are placed in microbeakers for image capture.

Figure 10 shows the measurement curve of the seven test samples. From these we obtain the angle that corresponds to the minimum intensity. Using the Equation 4, we find the corresponding refractive indices. Table 1 shows the value for each of the samples. Notice that the estimated refractive index values match well with the actual values. The mean error for the minimum intensity value estimate is 0.0142, the maximum error is 0.0242 and the minimum is 0.0066. This error is small and is well within an acceptable range.

Using the same measurement curves of the refractive index standards, we test the non-linear fitting algorithms. The

[7]These liquids belong to the AAA, AA, A, and B series of liquids from Cargille Labs. The refractive index liquids with n higher than 1.7, which belong to the H, EH, FH and the GH series contain toxic chemicals and are hazardous. Hence we limit the choice of liquids to the AAA, AA, A and the B series.

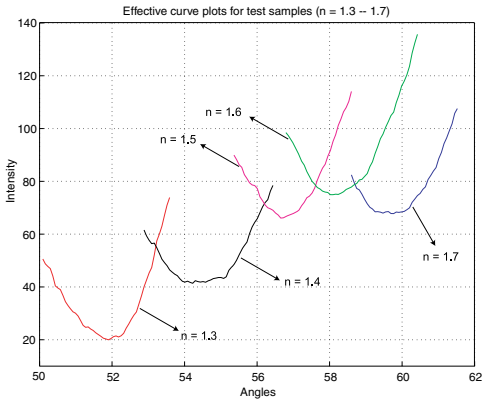

Figure 10. Measurement curves for samples with n ranging from 1.3 - 1.7 with intervals of 0.1. We see that as n increases, the position of the minimum intensity (Brewster angle) shifts to the right. Each curve is at different intensity levels. This depends on the reflectivity property of the test samples. The scaling and shifting done while carrying out non-linear curve fitting compensates for this non-uniform intensity level.

Sample	Ideal Refractive index (Known)	Estimated Refractive Index
Water	1.33	1.3222
Glass	1.517	1.5458
Ref. Index liquid 1	1.3	1.2799
Ref. Index liquid 2	1.4	1.4071
Ref. Index liquid 3	1.5	1.5224
Ref. Index liquid 4	1.6	1.6066
Ref. Index liquid 5	1.7	1.7113

Table 1. Results of minimum intensity estimate.

results for the seven samples found using this method are shown in Table 2. Here again, we see that the estimates are close the known values. The mean error for this estimation technique is 0.0171 with the maximum error is 0.0316 and minimum error is 0.0065. The plots for the experiments and the nonlinear-fitting results are shown in Figure 11.

7. Conclusion and Summary

We have presented the concept of reflectance coding using Brewster angles and we have developed a multiview imaging method to detect unknown Brewster angles. These methods provide a novel mechanism of watermarking that

Sample	Ideal Refractive index (Known)	Estimated Refractive Index
Water	1.33	1.2984
Glass	1.517	1.5263
Ref. Index liquid 1	1.3	1.2716
Ref. Index liquid 2	1.4	1.4065
Ref. Index liquid 3	1.5	1.5221
Ref. Index liquid 4	1.6	1.6139
Ref. Index liquid 5	1.7	1.7078

Table 2. Results of the nonlinear curve fitting estimate.

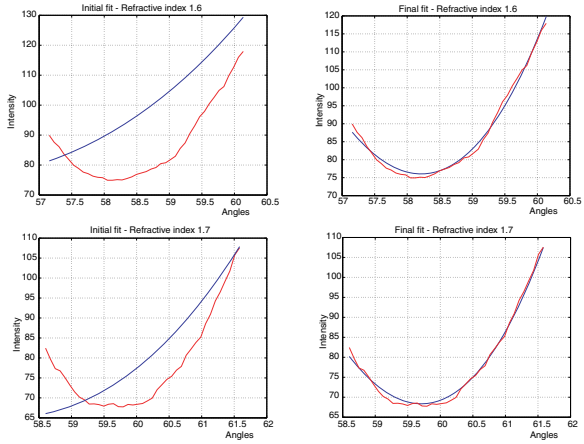

Figure 11. The estimates of the refractive indices of samples using the non-linear curve fitting techniques is shown in this figure. These plots are for refractive indices 1.6 and 1.7. The final estimated refractive indices for these are 1.6139 (for the 1.6 refractive index sample) and 1.7078 (for the 1.6 refractive index sample). The plots on the left are the initial estimates of the refractive index plotted along with the measurement curve. The plots on the right correspond to the same refractive index sample but are for the final estimate. We see that for each sample we get an ideal curve that fits very closely with the measurement curve at the end of the estimation process.

has significant advantages over existing methods for security purposes. The key novelty in our measurement approach is that the imaging does not require a device to step through detection and illumination angles. Multi-angle illumination and observation allows a simple imaging procedure. Furthermore, the exact orientation of the sample need not be known allowing for imaging in non-lab conditions. The device enables reading of transparent watermarks with

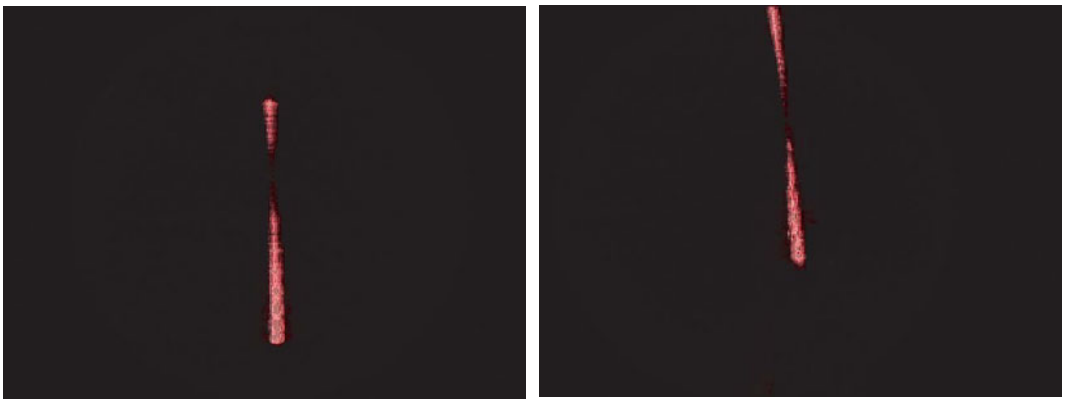

(a) (b)

Figure 12. Images are shown for glass (left) and clear lacquer (right) samples. The shift in the minimum intensity area is clearly visible. The refractive index for lacquer, which is around 1.42 has it minimum at a higher position than the glass sample, which has a refractive index of 1.517. This corresponds to the clear lacquer having a lower Brewster angle compared to glass.

information coded in a spatial variation of refractive index. The spatial variation of refractive index is invisible to the human eye but can be detected readily with this device.

References

[1] K. J. Dana, "BRDF/BTF measurement device," International Conference on Computer Vision **2**, 460–6 (2001).

[2] K. J. Dana and J. Wang, "Device for convenient measurement of spatially varying bidirectional reflectance," Journal of the Optical Society of America A **21**, 1–12 (2004).

[3] A. C. Traub and H. Osterberg, "Brewster angle apparatus for thin film index measurements," Journal of the Optical Society of America **47**(62) (1957).

[4] F. Abeles, "Methods for determining optical parameters of thin films," Progress in Optics **2**, 249–288 (1963).

[5] M. Hacskaylo, "Determination of the refractive index of thin film dielectric films," Journal of the Optical Society of America **54** (1964).

[6] Q. H. Wu and I. Hodgkinson, "Precision of Brewster-angle methods for optical thin films," Journal of the Optical Society of America A **10**(9) (1993).

[7] P. Logofatu, D. Apostol, V. Damian, I. Iordache, M. Bojan, and R. Muller, "Abeles method revisited," Applied Optics (2006).

[8] S. Henon and J. Meunier, "Microscope at the Brewster angle: direct observation of first-order phase transitions in monolayers," Rev. Sci. Instrum. **62**, 936 (1991).

[9] D. Hoenig and D. Moebius, "Direct visualization of monolayers at the air-water interface by Brewster Angle Microscopy," J. Phys. Chem. **95**, 4590–4592 (1991).

[10] C. Lheveder, S. Henon, R. Mercier, G. Tissot, P. Fournet, and J. Meunier, "A new Brewster angle microscope," Rev. Sci. Insts **69**, 1446 (1998).

[11] A. Y. Benbasat, "A Survey of Current Optical Security Techniques," MIT Media Lab Research Report (1999).

[12] J. Haslop, "Security Printing Techniques," Optical Document Security (1993).

[13] M. Gale, "Replication Technology for Holograms and Diffactive Optical Elements," Journal of Imaging Science and Technology **41**(3), 211–220 (1997).

[14] S. McGrew, "Hologram Counterfeiting: Problems and Solutions," SPIE Proceedings **1210**, 66–76 (1990).

[15] R. van Renesse, "Optical inspection techniques for security instrumentation," Proceedings of the SPIE, Optical Security and Counterfeit Deterrence Techniques **2659**, 159–167 (1996).

[16] R. L. van Renesse, *Optical Document Security* (Artech House, 1994).

[17] K. K. M. Gale and R. Morf, "Zero-order diffraction microstructures for security application," SPIE Proceedings **1210**, 83–89 (1990).

[18] R. E. Schafrik and S. E. Church, "Protecting the Greenback," Scientific American (1995).

[19] F. E. Boas, "How to make an unforgeable document," Harvard Science Review pp. 10–12 (1998).

[20] B. E. A. Saleh and M. C. Teich, *Fundamentals of Photonics* (John Wiley and Sons Inc., 1991).

[21] M. D. Grossberg and S. K. Nayar, "High Dynamic Range from Multiple Images: Which Exposures to Combine," ICCV Workshop on Color and Photometric Methods in Computer Vision (CPMCV) (2003).